Coexistence of superconductivity and ferromagnetism in P-doped EuFe$_2$As$_2$

S. Nandi,[1,2,*] W. T. Jin,[1,2] Y. Xiao,[1] Y. Su,[2] S. Price,[1] D. K. Shukla,[3,4] J. Strempfer,[3] H. S. Jeevan,[5]
P. Gegenwart,[5] and Th. Brückel[1,2]

[1]*Jülich Centre for Neutron Science JCNS and Peter Grünberg Institut PGI, JARA-FIT,
Forschungszentrum Jülich GmbH, D-52425 Jülich, Germany*
[2]*Jülich Centre for Neutron Science JCNS, Forschungszentrum Jülich GmbH, Outstation at MLZ,
Lichtenbergstraße 1, D-85747 Garching, Germany*
[3]*Deutsches Elektronen-Synchrotron DESY, D-22607 Hamburg, Germany*
[4]*UGC DAE Consortium for Scientific Research, Khandwa Road, Indore 01, India*
[5]*I. Physikalisches Institut, Georg-August-Universität Göttingen, D-37077 Göttingen, Germany*
(Received 23 October 2013; revised manuscript received 20 December 2013; published 23 January 2014)

The magnetic structure of the Eu^{2+} moments in the superconducting EuFe$_2$(As$_{1-x}$P$_x$)$_2$ sample with $x = 0.15$ has been determined using element-specific x-ray resonant magnetic scattering. Combining magnetic, thermodynamic, and scattering measurements, we conclude that the long-range ferromagnetic order of the Eu^{2+} moments aligned primarily along the **c** axis coexists with the bulk superconductivity at zero field. At an applied magnetic field $\geqslant 0.6$ T, superconductivity still coexists with the ferromagnetic Eu^{2+} moments, which are polarized along the field direction. We propose a spontaneous vortex state for the coexistence of superconductivity and ferromagnetism in EuFe$_2$(As$_{0.85}$P$_{0.15}$)$_2$.

I. INTRODUCTION

The discovery of the iron-based superconductors [1], a few years ago, has stimulated tremendous research interests worldwide in unconventional high-T_C superconductivity [2]. Most of the research on the Fe-based superconductors has focused on mainly four systems: (1) the quaternary "1111" systems, RFeAsO$_{1-x}$F$_x$ (R = La, Nd, Sm, or Pr, etc.) with T_C as high as 56 K [1,3–5], (2) the ternary "122" systems, AFe$_2$As$_2$ (A = Ba, Ca, Sr, or Eu, etc.) with T_C up to 38 K [6–8], (3) the binary "11" system (e.g., FeSe) [9] with $T_C \approx 18$ K, and (4) the ternary "245" systems, A_2Fe$_4$Se$_5$ (A = K, Rb, Cs) with $T_C \approx 30$ K [10]. Superconductivity can be achieved in all the above compounds in different ways, for example, either by electron or hole doping in the Fe-As layers [11,12] or by isovalent substitution [13–15]. Internal chemical pressure by isovalent substitution of arsenic with phosphorus [14,15] or external hydrostatic pressure can also give rise to superconductivity [16,17].

EuFe$_2$As$_2$ is an interesting member of the "122" family since the A site is occupied by Eu^{2+}, which is an S-state rare-earth ion possessing a $4f^7$ electronic configuration with the electron spin $S = 7/2$ [18]. EuFe$_2$As$_2$ exhibits a spin density wave (SDW) transition in the Fe sublattice concomitant with a structural phase transition at 190 K. In addition, Eu^{2+} moments order in an A-type antiferromagnetic (AFM) structure at 19 K (ferromagnetic layers ordered antiferromagnetically along the **c** axis) [19–21]. Superconductivity can be achieved in this system by substituting Eu with K or Na (see Refs. [7,22]), or As with P (see Ref. [23]), and upon application of external pressure (see Refs. [16,17,24]).

Superconductivity and magnetism are two antagonistic phenomena since the superconducting state expels external magnetic flux. Nevertheless, superconductivity in the pnictides and cuprates is always found in close proximity to an antiferromagnetic order and the superconducting pairing is believed to be mediated by the antiferromagntic spin fluctuations [2]. Most surprising is the coexistence of ferromagnetism and superconductivity as recently proposed by many groups for the P-doped EuFe$_2$As$_2$ samples [25–29]. Based on Mössbauer studies on superconducting polycrystalline samples, Nowik *et al.* [27] concluded that the Eu^{2+} moments are aligned ferromagnetically along the **c** axis with a possible tilting angle of 20° from the **c** axis. Zapf *et al.* also [28] concluded based on macroscopic measurements that the Eu^{2+} moments in EuFe$_2$(As$_{1-x}$P$_x$)$_2$ order in a canted A-type antiferromagnetic structure with the spin component along the **c** direction being ferromagnetically aligned. The small in plane component of the Eu^{2+} moments in the A-type AFM structure undergoes a spin glass transition where the moments between the layers are decoupled [29].

For a magnetic superconductor with rare-earth moments, several theoretical studies claim that the superconductivity can coexist with several forms of the magnetic states, namely, (a) "cryptoferromagnetism" (which is a ferromagnetic state with small domains, smaller than the superconducting coherence length) [30], (b) transverse amplitude modulated collinear antiferromagnetic structure, (c) spiral antiferromagnetic structure, or (d) with a spontaneous vortex state of the magnetic moments. A spontaneous vortex state or a self-induced vortex state is a new state of matter in which the two competing orders, superconductivity and ferromagnetism, coexist due to the lower free energy of the combined states compared to the individual ones [31]. The pure ferromagnetic state is least preferred. These results clearly show the importance of the alignment for the rare-earth moments in the superconducting samples.

To the best of our knowledge, for the superconducting EuFe$_2$(As$_{1-x}$P$_x$)$_2$ single-crystal samples, direct microscopic evidence for the proposed ferromagnetic and/or antiferromagnetic structure is still lacking. Due to the strong neutron absorption of Eu together with the small sample mass of the

P-doped single crystals, the magnetic structure determination in EuFe$_2$(As$_{1-x}$P$_x$)$_2$ via neutron diffraction is considerably more challenging than that of other members of the new superconductors. The only attempt was made on a powder sample of the nonsuperconducting EuFe$_2$P$_2$ where it was concluded that the Eu^{2+} moments order ferromagnetically with a canting angle of 17° from the **c** axis [32]. Here, we report on the first element-specific x-ray resonant magnetic scattering (XRMS) studies of the superconducting EuFe$_2$(As$_{1-x}$P$_x$)$_2$ to explore the details of the magnetic structure of the Eu^{2+} moments. Our resonant scattering experiments show that the Eu^{2+} moments order ferromagnetically along the **c** axis at zero field and undergo a transition into a field-induced ferromagnetic state along the applied magnetic field direction for applied magnetic fields $\geqslant$0.6 T. Both the zero and applied magnetic field ferromagnetic order of the Eu^{2+} moments coexist with the bulk superconductivity.

II. EXPERIMENTAL DETAILS

Single crystals of EuFe$_2$(As$_{1-x}$P$_x$)$_2$ with $x = 0.05$ and $x = 0.15$ were grown using FeAs flux [33]. For the scattering measurements and for the superconducting composition $x = 0.15$, an as-grown right isosceles triangular shaped single crystal with a base of approximately 2 mm and a thickness of 0.1 mm was selected. The *same* crystal was used for all the macroscopic characterizations presented in this communication. For the nonsuperconducting $x = 0.05$ sample, a crystal of approximate dimensions of $2 \times 2 \times 0.1$ mm^3 was chosen. The surface of both single crystals were perpendicular to the c axis. The XRMS experiments were performed at the Eu L_3 edge at beamline P09 at the PETRA III synchrotron at DESY [34]. The incident radiation was linearly polarized parallel (π polarization) and perpendicular (σ polarization) to the horizontal and vertical scattering planes for the 15% and 5% doped samples, respectively. The spatial cross section of the beam was 0.2 (horizontal) $\times$0.05 (vertical) mm^2. Copper Cu (2 2 0) was used at the Eu L_3 absorption edge as a polarization and energy analyzer to suppress the charge and fluorescence background relative to the magnetic scattering signal. The sample was mounted at the end of the cold finger of a cryomagnet with [2 1 0]$_T$-[0 0 1]$_T$ plane coincident with the scattering plane for the 15% doped sample. The magnetic field was applied along the [1 $\bar{2}$ 0] direction, which is perpendicular to the scattering plane. The 5% doped sample was measured inside a closed cycle Displex cryogenic refrigerator with [1 1 0]$_T$-[0 0 1]$_T$ as the scattering plane. Measurements at P09 were performed at temperatures between 5 and 180 K. For convenience, we will use tetragonal (T) notation unless otherwise specified.

III. EXPERIMENTAL RESULTS

A. Macroscopic characterizations

Figures 1(a)–1(b) and 1(c)–1(d) show magnetic susceptibility (*M-T*) and isothermal magnetization (*M-H*) of the $x = 0.15$ sample, respectively, measured for magnetic fields parallel and perpendicular to the c axis using a Quantum Design (SQUID) magnetometer. Zero-field cooled magnetization becomes negative for both field directions at
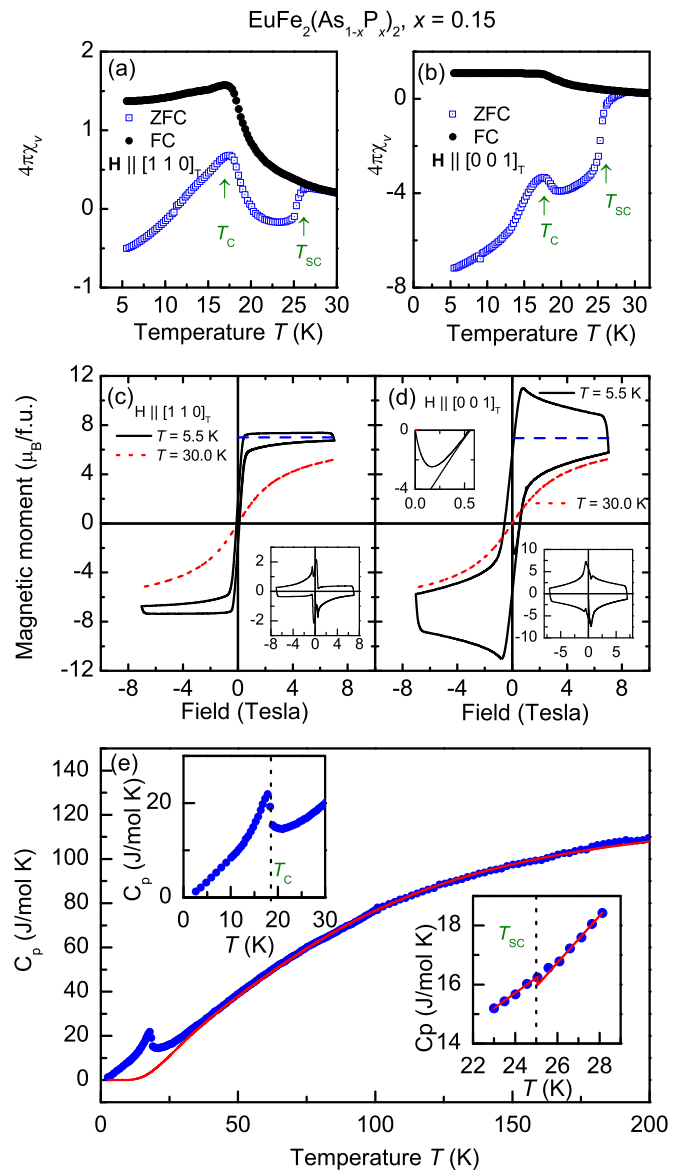

FIG. 1. (Color online) (a) and (b) Temperature dependencies of the magnetic susceptibility measured on heating of the zero-field cooled (ZFC) and field cooled (FC) sample at an applied magnetic field of 1 mT along the crystallographic [1 1 0]$_T$ and [0 0 1]$_T$ directions, respectively. (c) and (d) *M-H* curves for magnetic fields parallel and perpendicular to the **c** axis at $T = 5$ K (below magnetic and superconducting transitions) and 30 K (above superconducting and magnetic transitions). Horizontal dashed lines in both figures denote a fully saturated moment of Eu^{2+}. Lower insets for both figures show the hysteresis curves after subtraction of the ferromagnetic contribution as described in the text. The upper inset of Fig. 1(d) shows details of the *M-H* dependence in the low-field region. (e) Temperature dependence of the specific heat. Upper and lower insets show details near the magnetic ordering of the Eu^{2+} and the superconducting transition, respectively. The solid curve represents the fit using Debye and Einstein contributions for the lattice part of the specific heat. The lattice part was subtracted from the total heat capacity to calculate the entropy release at T_C.

$T_{SC} = 25$ K, signifying a superconducting transition at this temperature. Upon cooling towards the onset of Eu^{2+} ordering

at $T_C = 19$ K, the superconducting signal is first weakened, before it becomes more pronounced at temperatures below T_C. Superconductivity wins over the Eu^{2+} magnetism if temperature is lowered further. The diamagnetic volume susceptibility for the magnetic field parallel to the [1 1 0] direction (in this direction demagnetization correction is small [35]) is greater than -0.5 indicating bulk superconductivity [51]. Effective diamagnetic susceptibility close to -1 for the ZFC curve provides an upper limit of superconducting volume fraction of 100%. Figures 1(c) and 1(d) show hysteresis loops at $T = 5$ and 30 K for the two field directions. The observed hysteresis curves look different than a type II nonmagnetic superconductor. However, a jump in magnetization, which is typical for a type-II superconductor, is clearly observed at 7 T magnetic field between the field increasing and decreasing cycles. To understand the atypical hysteresis curve, we assume a ferromagnetic contribution of the Eu^{2+} moments at an applied magnetic field H (in Tesla) by

$$
\begin{aligned}
m_{Eu} &= (7.0/0.5) \times H\,\mu_B, \quad \text{for} \quad |H| \leqslant 0.5 \\
&= 7.0 \times H/|H|\,\mu_B, \quad \text{for} \quad |H| \geqslant 0.5,
\end{aligned}
\tag{1}
$$

since very little hysteresis was observed for the ferromagnetic end member $EuFe_2P_2$ [36]. Lower insets to Figs. 1(c) and 1(d) show magnetization after subtraction of the ferromagnetic contribution from the Eu^{2+} moments according to Eq. (1). The hysteresis curves after subtraction look very similar to the other Fe based superconductors [12,37]. The jump at 7-T magnetic field is consistent with Bean's critical state model together with Lenz's law [38–40]. Reversal of the direction of change of applied field as at 7 T does not remove the specimen from the critical state but merely reverses locally the direction of the critical current according to Lenz's law. Therefore magnetization measurements strongly hint towards a ferromagnetic superconductor in an applied magnetic field. The heat capacity of the same single crystal was measured using a Quantum Design physical property measurement system (PPMS) and is shown in Fig. 1(e). Specific heat data show a clear phase transition at $T_C = 19$ K indicating the onset of the Eu^{2+} magnetic order. A specific heat jump at T_{SC} is clearly visible and amounts to $\Delta C \approx 350$ mJ/mol K, which is slightly less but of the same order of magnitude as that observed for the K-doped $BaFe_2As_2$ system [41]. Due to the difficulties in determination of ΔC as well as "γ" as a result of large magnetic contribution at low temperatures, it will be hugely erroneous to estimate the value of $\Delta C/(\gamma T_{SC})$ and make comparison with other nonmagnetic iron-based superconductors. Heat capacity measurement down to mK temperature range is needed to correctly estimate the value of γ. The entropy release associated with the magnetic order of the Eu^{2+} moments amounts to 17.1 J/mol K, which is equal to 99% of the expected theoretical value $R\ln(2S + 1)$ for Eu^{2+} moments with spin $S = 7/2$. Therefore the specific heat measurement indicates that substantial volume of the sample, if not 100%, contributes to both the superconductivity and magnetic order of the Eu^{2+} moments. Moreover, the full moment of Eu^{2+} is completely ordered at the single phase transition temperature T_C of 19 K.

B. X-ray resonant magnetic scattering

To determine whether there is a structural phase transition, as observed in the parent compound $EuFe_2As_2$, $(\xi\ \xi\ 0)_T$ scans were performed through the tetragonal $(2\ 2\ 8)_T$ Bragg reflection as a function of temperature. The inset to Fig. 2(a) shows a subset of $(\xi\ \xi\ 0)_T$ scans through the $(2\ 2\ 8)_T$ reflection for the 15% doped sample as the sample was cooled through $T_S = 49 \pm 1$ K. The splitting of the $(2\ 2\ 8)_T$ Bragg reflection into orthorhombic (O) $(4\ 0\ 8)_O$ and $(0\ 4\ 8)_O$ Bragg reflections below T_S is consistent with the structural transition, from space group $I4/mmm$ to $Fmmm$, with a distortion along the [1 1 0] direction. As the sample is cooled further, the orthorhombic splitting (δ) increases down to $T = 30 \pm 1$ K as can be seen from Fig. 2(a). Near T_{SC}, δ shows a local minimum due to the competition between superconductivity and ferromagnetism. Lowering the temperature below T_C results in a smooth decrease in δ, reminiscent of that observed in the superconducting $Ba(Fe_{1-x}Co_x)_2As_2$ samples [42]. The nonsuperconducting 5% doped sample undergoes a similar structural phase transition at $T_S = 165 \pm 1$ K but without any decrease of the orthorhombic distortion for lower temperatures.

Below $T_C = 20$ K, a magnetic signal was observed when the x-ray energy was tuned through the Eu L_3 edge at reciprocal lattice points identical to those of the charge reflections, indicating the onset of the Eu^{2+} magnetic order at the magnetic propagation vector $\boldsymbol{\tau} = (0\ 0\ 0)$. Figure 2(b) depicts the temperature evolution of the (2 1 7) reflection measured at the Eu L_3 edge at resonance ($E = 6.973$ keV). A variation of the magnetic intensity with temperature was only observed in the $\pi \rightarrow \sigma'$ scattering channel, whereas the $\pi \rightarrow \pi'$ scattering channel shows no discernible temperature dependence. The transition temperature is similar to that observed in the parent $EuFe_2As_2$ compound and consistent with the results presented in Fig. 1. Figure 2(c) shows temperature dependence of the same (2 1 7) reflection in an applied magnetic field of 0.5 T along the [1 $\bar{2}$ 0] direction in both scattering channels. It is interesting to see that the temperature dependence appears in the opposite scattering channel compared to the zero field and indicates a possible flop of the magnetic moment in an applied magnetic field which will be discussed later. The transition temperature is increased from 19 K at zero field to 29 K at 0.5 T.

To confirm the resonant magnetic behavior of the peaks, we performed energy scans at the Eu L_3 absorption edge as shown in Fig. 3. We note that for the (2 1 7) reflection charge and magnetic peak coincide. An investigation of the magnetic signal which is five to six orders of magnitude weaker than the Thomson charge scattering requires significant reduction of the charge background. The charge background can be reduced significantly for a reflection with scattering angle close to 90° [43,44]. Since the (2 1 7) reflection has a scattering angle of $\sim$94.5° at the Eu L_3 edge, the investigation of the magnetic signal seems feasible for this reflection. Figure 3(b) shows an energy scan through the (2 1 7) reflection after subtracting the nonmagnetic background at $T = 22$ K. A clear resonance enhancement can be seen close to the Eu L_3 edge. A similar resonance enhancement can be observed in the $\pi \rightarrow \pi'$ scattering channel in an applied magnetic field of 3 T. In both energy scans, the resonance peaks appear at and above the Eu L_3 absorption edge, indicating the dipole
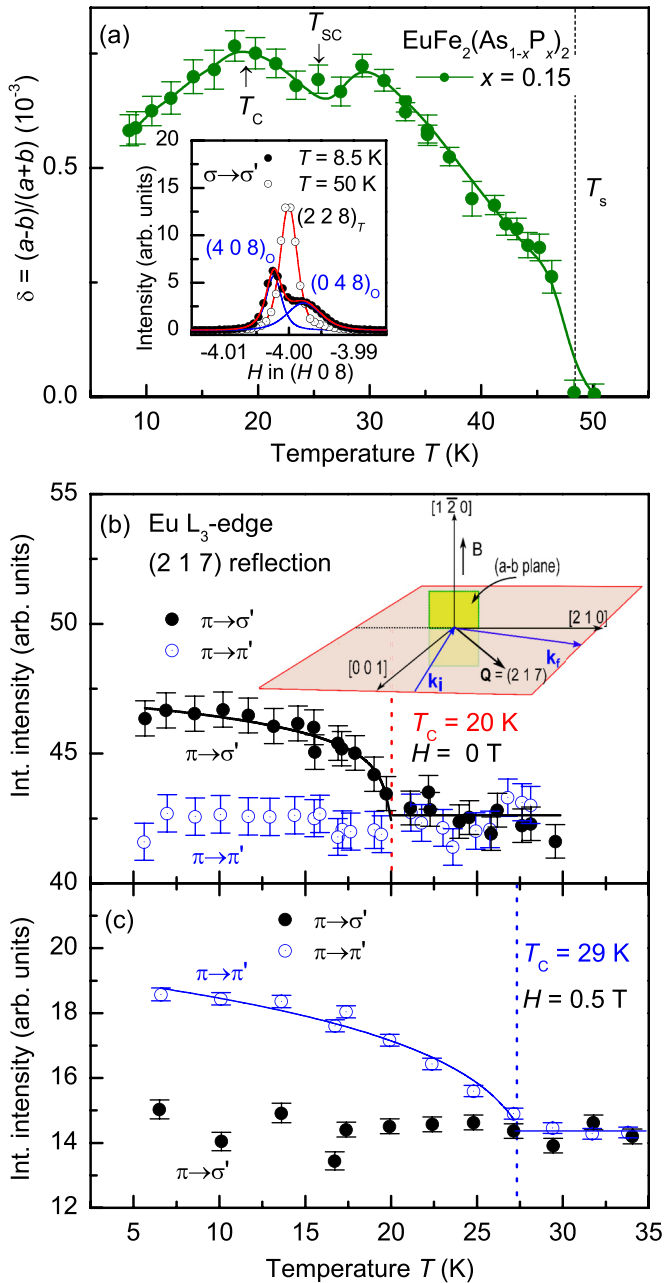
FIG. 2. (Color online) (a) Temperature dependence of the orthorhombic distortion for the $x = 0.15$ sample. The inset shows $(\xi\ \xi\ 0)_T$ scans through the $(2\ 2\ 8)_T$ position above and below the structural phase transition. The lines represent fits to the data using either one (red) or two (blue) Lorentzian squared peaks. (b) Temperature dependence of the (2 1 7) reflection in both the $\pi \rightarrow \sigma'$ and $\pi \rightarrow \pi'$ scattering geometries at zero filed. The schematic shows the used scattering geometry. (c) Same as (b) but in an applied magnetic field of 0.5 T. The temperature dependencies were measured at the peak energy ($\sim$6.973 keV) of the resonance enhancement observed in the energy scans.

nature of the transition. Figure 3(d) shows energy scans through the antiferromagnetic (0 0 3) position, expected for an A-type AFM structure, for the 15% doped sample in the $\pi \rightarrow \sigma'$ scattering channel. For comparison, we also show the energy scan through the (0 0 9) position in Fig. 3(e) for
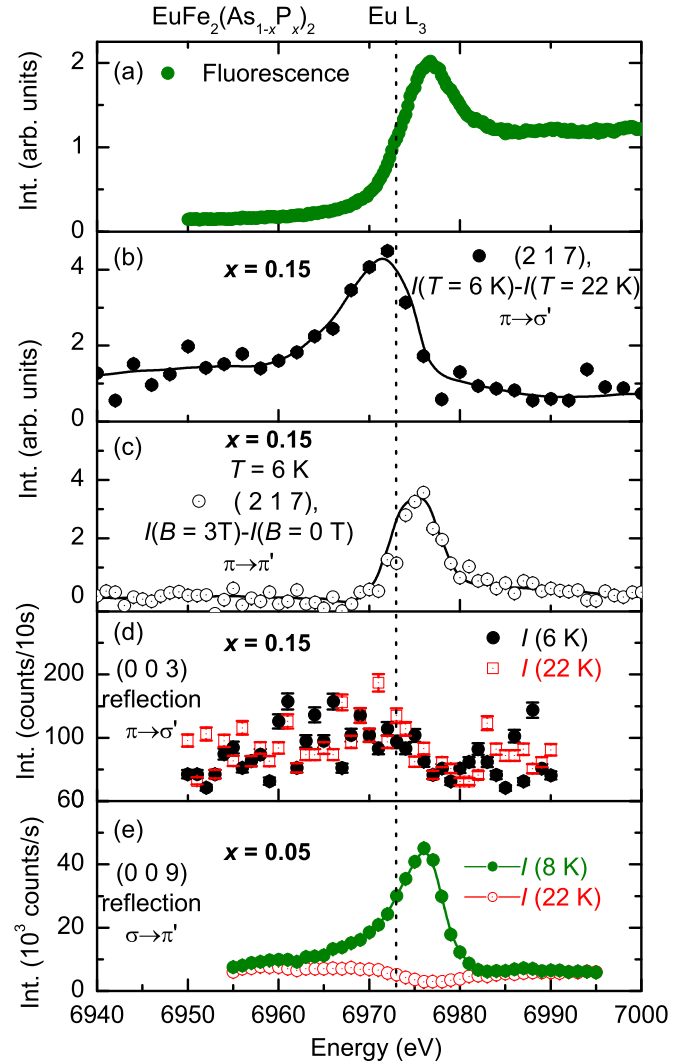

FIG. 3. (Color online) (a) Energy scan of the fluorescence yield. The dashed line depicts the Eu L_3 absorption edge as determined from the inflection point of the fluorescence yield. (b) and (c) Energy scans for the (2 1 7) reflection after subtraction of the nonmagnetic background at high temperature for (b) and at zero magnetic field for (c). (d) and (e) Energy scans through the antiferromagnetic (0 0 3) and (0 0 9) positions for the 15% and 5% samples, respectively. Lines serve as guides to the eye.

the 5% doped sample measured under similar conditions. A strong antiferromagnetic signal was observed for the 5% doped sample at the A-type AFM position, which is in contrast to the 15% doped sample where no magnetic signal was observed. Therefore the proposed A-type AFM structure [28] could not be confirmed for the superconducting 15% P-doped sample. This might be due to the small moment in the A-type AFM structure together with the glassy freezing of the in-plane component as suggested by Ref. [29].

C. Magnetic structure in zero and applied magnetic fields

We now turn to the determination of the magnetic moment configuration for the Eu^{2+} moments in the zero and applied magnetic fields. For the crystallographic space group *Fmmm*

TABLE I. Basis vectors for the space group *Fmmm* with $\boldsymbol{\tau} = (0\ 0\ 0)$. The decomposition of the magnetic representation for the Eu site at $(0\ 0\ 0)$ is $\Gamma_{\text{Mag}} = 0\Gamma_1^1 + 0\Gamma_2^1 + 1\Gamma_3^1 + 0\Gamma_4^1 + 1\Gamma_5^1 + 0\Gamma_6^1 + 1\Gamma_7^1 + 0\Gamma_8^1$.

| | | BV components | | | Magnetic Intensity (2 1 7) | |
| | | | | | | |
IR	Atom	$m_{\parallel a}$	$m_{\parallel b}$	$m_{\parallel c}$	$\pi \to \sigma'$	$\pi \to \pi'$
Γ_3	1	1	0	0	Yes	Yes
Γ_5	1	0	1	0	Yes	Yes
Γ_7	1	0	0	1	Yes	No

and $\boldsymbol{\tau} = (0\ 0\ 0)$, three independent magnetic representations (MRs) are possible [45]. Here, we note that only ferromagnetic structures with magnetic moments along the three crystallographic directions **a**, **b**, **c** are allowed by symmetry. No

antiferromagnetic structure with $\boldsymbol{\tau} = (0\ 0\ 0)$ is possible in this case for symmetry reasons. All the MRs along with the calculated intensities for different polarization geometries are listed in Table I.

The resonant scattering of interest, at the Eu L_3 absorption edge, is due to electric dipole transitions between the core $2p$ states and the $5d$ conduction bands. The $5d$ bands are spin polarized through the exchange interaction with the magnetic $4f$ electrons. The resonant magnetic scattering cross-section for the dipole resonance can be written as [46]

$$f_{nE1}^{\text{XRMS}} = [(\hat{\epsilon}' \cdot \hat{\epsilon})F^{(0)} - i(\hat{\epsilon}' \times \hat{\epsilon}) \cdot \hat{z}_n F^{(1)}$$
$$+ (\hat{\epsilon}' \cdot \hat{z}_n)(\hat{\epsilon} \cdot \hat{z}_n)F^{(2)}], \qquad (2)$$

where $\hat{z}_n$ is a unit vector in the direction of the magnetic moment of the nth ion. Here, $\hat{\epsilon}$ and $\hat{\epsilon}'$ are the incident and scattered polarization vectors, and $F^{(i)}$'s are the terms
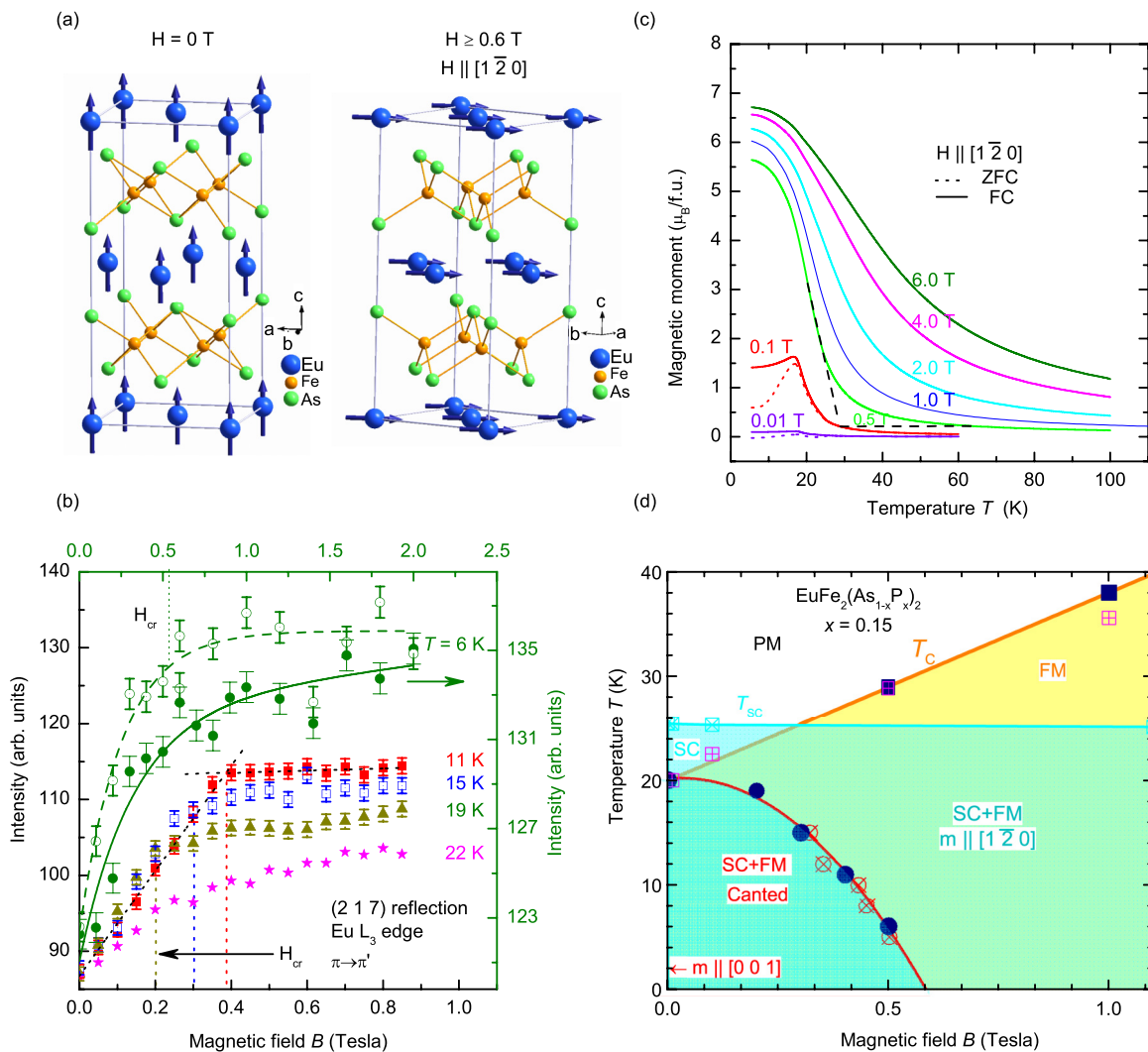

FIG. 4. (Color online) (a) Magnetic structures of the Eu^{2+} moments in zero and applied magnetic fields. Only the Eu^{2+} magnetic moments are shown. (b) Field dependence of the intensities of the (2 1 7) reflection measured in the $\pi \to \pi'$ scattering geometry after zero field cooling of the sample from 80 K. (c) Temperature dependence of the bulk magnetization at different applied magnetic fields along the [1 $\bar{2}$ 0] direction measured using an MPMS. (d) Magnetic phase diagram for the 15% doped sample constructed using magnetization and scattering measurements. Filled symbols are derived from the scattering measurement and the open symbols from M-T (square) and M-H (circles) measurements at different fields and temperatures, respectively. The transition temperatures, T_{SC} and T_{C}, at zero field are consistent with the published results of Ref. [33].

containing dipole matrix elements. The first term of Eq. (2) contributes to the charge Bragg peak as it does not contain any dependence on the magnetic moment. The other two terms are sensitive to the magnetic moment. For a ferromagnetic structure, in general, all terms contribute to the scattering at every Bragg reflection. However, for the Eu^{2+} ions with spin only magnetic moment, the spherical symmetry of the spin-polarized $5d$ band ensures that the $F^{(2)}$ term is zero [47]. For the $\pi \rightarrow \sigma'$ scattering geometry, the scattering amplitude from Eq. (2) can be written in a simplified form as $f \propto \mathbf{k}_i \cdot \boldsymbol{\mu}$ [48], where $\mathbf{k_i}$ and $\boldsymbol{\mu}$ are the wave vector of the incoming photons and the magnetic moment, respectively. Clearly, the magnetic signal is sensitive to the component of the ordered moment in the scattering plane, i.e., a/b and c components. For the $\pi \rightarrow \pi'$ scattering geometry, the scattering amplitude can be written as $f \propto (\mathbf{k}_i \times \mathbf{k}_f) \cdot \boldsymbol{\mu}$ [48], where $\mathbf{k_f}$ is the wave vector of the outgoing photons. Therefore, in the $\pi \rightarrow \pi'$ scattering geometry, the magnetic signal is sensitive to the component of the ordered moment perpendicular to the scattering plane, i.e., only a/b components. Since, no magnetic signal was observed in the $\pi \rightarrow \pi'$ scattering channel at zero field [see Fig. 2(b)], we conclude that the magnetic moments are aligned primarily along the **c** axis. For the applied magnetic field the situation is reversed. The magnetic signal is observed only in the $\pi \rightarrow \pi'$ scattering channel [see Fig. 2(c)] indicating the magnetic moments are in the a-b plane. It is most likely that the magnetic moments are along the applied filed direction, i.e., along the $[1 \, \bar{2} \, 0]$ direction. The determined magnetic structures based on the polarization analysis of the scattered signal is presented in Fig. 4(a).

Having determined the magnetic structures in zero and applied magnetic fields, we have measured the field dependencies of the integrated intensity of the magnetic (2 1 7) reflection for several temperatures, which are presented in Fig. 4(b). A clear hysteresis can be seen from the increasing and decreasing field cycles at $T = 6$ K, which is typical for a ferromagnet. The critical field, H_{cr}, at which the field-induced phase transition occurs, has been determined from the intercept of the high- and low-field linear interpolation as shown for the $T = 11$ K measurement in Fig. 4(b). The field dependence of the ferromagnetic ordering temperature has been determined from the temperature dependence of the (2 1 7) reflection in the $\pi \rightarrow \pi'$ scattering geometry as shown in Fig. 2(c). Additionally, isothermal magnetization (*M-H*) at different temperatures (not shown) and temperature dependencies of magnetization (*M-T*) at different magnetic fields [see Fig. 4(c)] have been performed to verify the transition temperatures and critical fields obtained from scattering measurements. A combined phase diagram has been

constructed and is shown in Fig. 4(d). It can be seen that superconductivity coexists with strong ferromagnetic order of the Eu^{2+} moments for a large region of the phase diagram. For $B \leqslant 0.5$ T, the superconducting transition precedes the ferromagnetic transition, whereas the situation is reversed for magnetic fields higher than 0.5 T.

IV. DISCUSSION AND CONCLUSION

The most important result of the present study is the observation of strong ferromagnetic order of the Eu^{2+} moments coexisting with bulk superconductivity. Magnetization, specific heat, and temperature dependence of the structural distortion indicates bulk nature of the superconducting transition. In contrast to the previous studies, we got no indication of the proposed A-type AFM structure or a spiral magnetic order with propagation vector of the form $(0\ 0\ \tau)$ [52]. In the Fe-As based superconductors, it is believed that the superconducting carriers are in the Fe-As layers. Therefore, to understand the phenomena of coexistence, we have calculated the effective field due the Eu^{2+} moments at the Fe-As layers using dipole approximation. To a first approximation, the dipole field does not exceed 1 T, which is much less than the superconducting upper critical field H_{C2} (≈ 40 T) [2] but higher than the lower critical field H_{C1} (≈ 0.02–0.03 T) [12]. Since the internal field is between H_{C1} and H_{C2}, it is most likely that the $EuFe_2(As_{1-x}P_x)_2$ is in a spontaneous vortex state similar to which have been proposed in $Eu(Fe_{0.75}Ru_{0.25})_2As_2$ [49] and UCoGe superconductors [50]. At an applied magnetic field, it is most likely that the vortices in the zero-field state (along the c axis) will gradually change along the applied field direction, i.e., in the a-b plane.

In conclusion, the magnetic structure of the Eu moments in superconducting $EuFe_2(As_{1-x}P_x)_2$ with $x = 0.15$ has been determined using element specific x-ray resonant magnetic scattering. Combining magnetic, thermodynamic, and scattering measurements we conclude that the long-range ferromagnetic order of the Eu^{2+} moments aligned primarily along the **c** axis coexists with the bulk superconductivity. The proposed canted antiferromagnetic order or spiral order could not be confirmed in the superconducting sample. Additional measurements such as small angle neutron scattering is needed to confirm the existence of a spontaneous vortex state.

[1] Y. Kamihara, T. Watanabe, M. Hirano, and H. Hosono, J. Am. Chem. Soc. **130**, 3296 (2008).

[2] D. C. Johnston, Adv. Phys. **59**, 803 (2010).

[3] H. Takahashi, K. Igawa, K. Arii, Y. Kamihara, M. Hirano, and H. Hosono, Nature (London) **453**, 376 (2008).

[4] X. H. Chen, T. Wu, G. Wu, R. H. Liu, H. Chen, and D. F. Fang, Nature (London) **453**, 761 (2008).

[5] R. Zhi-An, L. Wei, Y. Jie, Y. Wei, S. Xiao-Li, L. Zheng-Cai, C. Guang-Can, D. Xiao-Li, S. Li-Ling, Z. Fang, and Z. Zhong-Xian, Chin. Phys. Lett. **25**, 2215 (2008).

[6] M. Rotter, M. Tegel, and D. Johrendt, Phys. Rev. Lett. **101**, 107006 (2008).

[7] H. S. Jeevan, Z. Hossain, D. Kasinathan, H. Rosner, C. Geibel, and P. Gegenwart, Phys. Rev. B **78**, 092406 (2008).

[8] K. Sasmal, B. Lv, B. Lorenz, A. M. Guloy, F. Chen, Y.-Y. Xue, and C.-W. Chu, Phys. Rev. Lett. **101**, 107007 (2008).

[9] F.-C. Hsu, J.-Y. Luo, K.-W. Yeh, T.-K. Chen, T.-W. Huang, P. M. Wu, Y.-C. Lee, Y.-L. Huang, Y.-Y. Chu, D.-C. Yan, and M.-K. Wu, Proc. Natl. Acad. Sci. USA **105**, 14262 (2008).

[10] J. Guo, S. Jin, G. Wang, S. Wang, K. Zhu, T. Zhou, M. He, and X. Chen, Phys. Rev. B **82**, 180520 (2010).

[11] A. Leithe-Jasper, W. Schnelle, C. Geibel, and H. Rosner, Phys. Rev. Lett. **101**, 207004 (2008).

[12] A. S. Sefat, R. Jin, M. A. McGuire, B. C. Sales, D. J. Singh, and D. Mandrus, Phys. Rev. Lett. **101**, 117004 (2008).

[13] W. Schnelle, A. Leithe-Jasper, R. Gumeniuk, U. Burkhardt, D. Kasinathan, and H. Rosner, Phys. Rev. B **79**, 214516 (2009).

[14] C. Wang, S. Jiang, Q. Tao, Z. Ren, Y. Li, L. Li, C. Feng, J. Dai, G. Cao, and Z.-an Xu, Europhys. Lett. **86**, 47002 (2009).

[15] S. Jiang, H. Xing, G. Xuan, C. Wang, Z. Ren, C. Feng, J. Dai, Z. Xu, and G. Cao, J. Phys.: Condens. Matter **21**, 382203 (2009).

[16] C. F. Miclea, M. Nicklas, H. S. Jeevan, D. Kasinathan, Z. Hossain, H. Rosner, P. Gegenwart, C. Geibel, and F. Steglich, Phys. Rev. B **79**, 212509 (2009).

[17] Y. Tokiwa, S.-H. Hübner, O. Beck, H. S. Jeevan, and P. Gegenwart, Phys. Rev. B **86**, 220505 (2012).

[18] R. Marchand and W. Jeitschko, J. Solid State Chem. **24**, 351 (1978).

[19] J. Herrero-Martín, V. Scagnoli, C. Mazzoli, Y. Su, R. Mittal, Y. Xiao, T. Brueckel, N. Kumar, S. K. Dhar, A. Thamizhavel, and L. Paolasini, Phys. Rev. B **80**, 134411 (2009).

[20] Y. Xiao, Y. Su, M. Meven, R. Mittal, C. M. N. Kumar, T. Chatterji, S. Price, J. Persson, N. Kumar, S. K. Dhar, A. Thamizhavel, and Th. Brueckel, Phys. Rev. B **80**, 174424 (2009).

[21] Y. Xiao, Y. Su, W. Schmidt, K. Schmalzl, C. M. N. Kumar, S. Price, T. Chatterji, R. Mittal, L. J. Chang, S. Nandi, and N. Kumar, S. K. Dhar, A. Thamizhavel, and Th. Brueckel, Phys. Rev. B **81**, 220406(R) (2010).

[22] Y. Qi, Z. Gao, L. Wang, D. Wang, X. Zhang, and Y. Ma, New J. Phys. **10**, 123003 (2008).

[23] Z. Ren, Q. Tao, S. Jiang, C. Feng, C. Wang, J. Dai, G. Cao, and Z. Xu, Phys. Rev. Lett. **102**, 137002 (2009).

[24] T. Terashima, M. Kimata, H. Satsukawa, A. Harada, K. Hazama, S. Uji, H. S. Suzuki, T. Matsumoto, and K. Murata, J. Phys. Soc. Jpn. **78**, 083701 (2009).

[25] G. Cao, S. Xu, Z. Ren, S. Jiang, C. Feng, and Z. Xu, J. Phys.: Condens. Matter **23**, 464204 (2011).

[26] A. Ahmed, M. Itou, S. Xu, Z. Xu, G. Cao, Y. Sakurai, J. Penner-Hahn, and A. Deb, Phys. Rev. Lett. **105**, 207003 (2010).

[27] I. Nowik, I. Felner, Z. Ren, G. H. Cao, and Z. A. Xu, J. Phys.: Condens. Matter **23**, 065701 (2011).

[28] S. Zapf, D. Wu, L. Bogani, H. S. Jeevan, P. Gegenwart, and M. Dressel, Phys. Rev. B **84**, 140503 (2011).

[29] S. Zapf, H. S. Jeevan, T. Ivek, F. Pfister, F. Klingert, S. Jiang, D. Wu, P. Gegenwart, R. K. Kremer, and M. Dressel, Phys. Rev. Lett. **110**, 237002 (2013).

[30] P. W. Anderson and H. Suhl, Phys. Rev. **116**, 898 (1959).

[31] H. S. Greenside, E. I. Blount, and C. M. Varma, Phys. Rev. Lett. **46**, 49 (1981).

[32] D. H. Ryan, J. M. Cadogan, S. Xu, Z. Xu, and G. Cao, Phys. Rev. B **83**, 132403 (2011).

[33] H. S. Jeevan, D. Kasinathan, H. Rosner, and P. Gegenwart, Phys. Rev. B **83**, 054511 (2011).

[34] J. Strempfer, S. Francoual, D. Reuther, D. K. Shukla, A. Skaugen, H. Schulte-Schrepping, T. Kracht, and H. Franz, J. Synchrotron Rad. **20**, 541 (2013).

[35] J. A. Osborn, Phys. Rev. **67**, 351 (1945).

[36] C. Feng, Z. Ren, S. Xu, S. Jiang, Z. Xu, G. Cao, I. Nowik, I. Felner, K. Matsubayashi, and Y. Uwatoko, Phys. Rev. B **82**, 094426 (2010).

[37] R. Prozorov, N. Ni, M. A. Tanatar, V. G. Kogan, R. T. Gordon, C. Martin, E. C. Blomberg, P. Prommapan, J. Q. Yan, S. L. Bud'ko, and P. C. Canfield, Phys. Rev. B **78**, 224506 (2008).

[38] C. P. Bean, Phys. Rev. Lett. **8**, 250 (1962).

[39] Y. B. Kim, C. F. Hempstead, and A. R. Strnad, Phys. Rev. **129**, 528 (1963).

[40] W. A. Fietz, M. R. Beasley, J. Silcox, and W. W. Webb, Phys. Rev. **136**, A335 (1964).

[41] N. Ni, S. L. Bud'ko, A. Kreyssig, S. Nandi, G. E. Rustan, A. I. Goldman, S. Gupta, J. D. Corbett, A. Kracher, and P. C. Canfield, Phys. Rev. B **78**, 014507 (2008).

[42] S. Nandi, M. G. Kim, A. Kreyssig, R. M. Fernandes, D. K. Pratt, A. Thaler, N. Ni, S. L. Bud'ko, P. C. Canfield, J. Schmalian, R. J. McQueeney, and A. I. Goldman, Phys. Rev. Lett. **104**, 057006 (2010).

[43] S. Nandi, Y. Su, Y. Xiao, S. Price, X. F. Wang, X. H. Chen, J. Herrero-Martin, C. Mazzoli, H. C. Walker, L. Paolasini, S. Francoual, D. K. Shukla, J. Strempfer, T. Chatterji, C. M. N. Kumar, R. Mittal, H. M. Rønnow, Ch. Rüegg, D. F. McMorrow, and Th. Brückel, Phys. Rev. B **84**, 054419 (2011).

[44] J. W. Kim, A. Kreyssig, P. Ryan, E. Mun, P. C. Canfield, and A. I. Goldman, Appl. Phys. Lett. **90**, 202501 (2007).

[45] A. S. Wills, Physica B **276–278**, 680 (2000).

[46] J. P. Hill and D. F. McMorrow, Acta Crystallogr. A **52**, 236 (1996).

[47] M. D. Hamrick, M.A. thesis, Rice University, 1990.

[48] S. Nandi, *Magnetic X-Ray Scattering* (Wiley, New York, 2012).

[49] W.-H. Jiao, Q. Tao, J.-K. Bao, Y.-L. Sun, C.-M. Feng, Z.-A. Xu, I. Nowik, I. Felner, and G.-H. Cao, Europhys. Lett. **95**, 67007 (2011).

[50] K. Deguchi, E. Osaki, S. Ban, N. Tamura, Y. Simura, T. Sakakibara, I. Satoh, and N. K. Sato, J. Phys. Soc. Jpn. **79**, 083708 (2010).

[51] χ_v is larger than the ideal value of -1. However, considering the ferromagnetic contribution of the Eu^{2+} (as found by the scattering measurements), the effective volume susceptibility due to the superconductivity (SC), $(\chi_v^{SC}) = \chi_{observed} - \chi_{Eu}^{Ferro}$, might be very close to -1. The observed ferromagnetic contribution for the nonsuperconducting ferromagnet $EuFe_2P_2$ [36] (in ZFC data) is the same order of magnitude as the $\chi_{observed}$ in the present case.

[52] Careful scans along [0 0 L] direction do not reveal any magnetic peak.